Sphingosine-1-phosphate induces Ca^2 signaling and CXCL1 release via TRPC6 channel in astrocytes.

AUTHOR(S):

Shirakawa, Hisashi; Katsumoto, Rumi; Iida, Shota; Miyake, Takahito; Higuchi, Takuya; Nagashima, Takuya; Nagayasu, Kazuki; Nakagawa, Takayuki; Kaneko, Shuji

CITATION:

Shirakawa, Hisashi ...[et al]. Sphingosine-1-phosphate induces Ca^2 signaling and CXCL1 release via TRPC6 channel in astrocytes.. Glia 2017, 65(6): 1005-1016

ISSUE DATE:

2017-06

URL:

http://hdl.handle.net/2433/241619

Sphingosine-1-phosphate induces Ca^{2+} signaling and CXCL1 release via TRPC6 channel in astrocytes

Hisashi Shirakawa[1], Rumi Katsumoto[1], Shota Iida[1], Takahito Miyake[1], Takuya Higuchi[1], Takuya Nagashima[1], Kazuki Nagayasu[1], Takayuki Nakagawa[2], and Shuji Kaneko[1]

[1]Department of Molecular Pharmacology, Graduate School of Pharmaceutical Sciences, Kyoto University

[2]Department of Clinical Pharmacology and Therapeutics, Kyoto University Hospital

Correspondence to:

Hisashi Shirakawa, PhD,

Department of Molecular Pharmacology, Graduate School of Pharmaceutical Sciences, Kyoto University

46-29 Yoshida-shimoadachi-cho, Sakyo-ku, Kyoto, 606-8501, Japan,

Tel: +81-75-753-4549, Fax: +81-75-753-4548; E-mail; shirakaw@pharm.kyoto-u.ac.jp

Running title: TRPC6 involvement in astrocytic CXCL1 release

The exact number of words in Abstract: 223; Introduction: 348; Materials and methods: 1527; Results: 1408; Discussion: 952; Legends: 949; Bibliography: 1391. Total words count: 7034. The number of figures: 6; tables: none.

Main points; Activation of G_q-coupled receptors $S1P_2$ and $S1P_3$ by S1P triggers Ca^{2+} influx through TRPC6, which results in MAPK activation and increased secretion of the proinflammatory or neuroprotective chemokine CXCL1 in astrocyte *in vitro*.

Key words: Astrocytes, Calcium signaling, Sphingosine 1-phosphate, TRP Channels, Chemokines

Abstract

A biologically active lipid, sphingosine-1-phosphate (S1P) is highly abundant in blood, and plays an important role in regulating the growth, survival, and migration of many cells. Binding of the endogenous ligand S1P results in activation of various signaling pathways via G protein-coupled receptors, some of which generates Ca^{2+} mobilization. In astrocytes, S1P is reported to evoke Ca^{2+} signaling, proliferation, and migration; however, the precise mechanisms underlying such responses in astrocytes remain to be elucidated. Transient receptor potential canonical (TRPC) channels are Ca^{2+}-permeable cation channels expressed in astrocytes and involved in Ca^{2+} influx after receptor stimulation. In this study, we investigated the involvement of TRPC channels in S1P-induced cellular responses. In Ca^{2+} imaging experiments, S1P at 1 μM elicited a transient increase in intracellular Ca^{2+} in astrocytes, followed by sustained elevation. The sustained Ca^{2+} response was markedly suppressed by $S1P_2$ receptor antagonist JTE013, $S1P_3$ receptor antagonist CAY10444, or non-selective TRPC channel inhibitor Pyr2. Additionally, S1P increased chemokine CXCL1 mRNA expression and release, which were suppressed by TRPC inhibitor, inhibition of Ca^{2+} mobilization, MAPK pathway inhibitors, or knockdown of the TRPC channel isoform TRPC6. Taken together, these results demonstrate that S1P induces Ca^{2+} signaling in astrocytes via G_q-coupled receptors $S1P_2$ and $S1P_3$, followed by Ca^{2+} influx through TRPC6 that could activate MAPK signaling, which leads to increased secretion of the proinflammatory or neuroprotective chemokine CXCL1.

Introduction

Astrocytes are the most abundant cells in the CNS and play diverse roles in the regulation of neuronal activity, vascular function, and gliotransmitter release [Mulligan and MacVicar, 2004; Khakh and Sofroniew, 2015; Verkhratsky et al., 2016]. By contrast, pathologically activated astrocytes have been reported to show astrogliosis, which can cause neuronal dysfunction in neurodegenerative diseases [Allaman et al., 2011; Sofroniew, 2009]. Although, astrocytes are electrically nonexcitable, they can be excited by Ca^{2+} signaling [Bazargani and Attwell, 2016; Fiacco and McCarthy, 2006; Rusakov, 2015].

Transient receptor potential canonical (TRPC) channels, Ca^{2+}-permeable nonselective cation channels, function as homo- or heterotetrameric channels and at least one of seven isoforms is expressed in almost every tissue where they facilitate voltage-independent Ca^{2+} entry in response to store depletion induced by receptor stimulation [Birnbaumer, 2009]. In astrocytes, several isoforms of TRPC channels play important roles in astrocytic Ca^{2+} responses induced by store depletion [Golovina, 2005], diacylglycerol activation [Grimaldi, 2006], mechanical stimulation or ATP [Beskina et al., 2007], and thrombin [Shirakawa et al., 2010].

Sphingosine-1-phosphate (S1P) is a biologically active sphingolipid that plays an important role in regulating the growth, survival and migration of mammalian cells [Brinkmann, 2007; Pyne and Pyne, 2010]. In astrocytes, S1P induces cellular proliferation [Malchinkhuu et al., 2003], morphological changes [Rouach et al., 2006], and cellular migration [Fischer et al., 2011]. Moreover, S1P induces expression of a variety of neurotrophic factors, such as GDNF [Yamagata et al., 2003], NGF [Furukawa et al., 2007] and cytokines, such as interleukin (IL) 1β and CCL2 [Zhou and Murthy, 2004] in astrocytes. Moreover, S1P activates the $G_{q/11}$ inositol

lipid/ Ca^{2+} signaling pathway in cortical astrocytes [Sorensen et al., 2003]. However, the precise molecular mechanisms underlying S1P-induced Ca^{2+} responses and functional changes in astrocytes remain unknown. Thus, we focused on and investigated the involvement of TRPC channels in S1P-induced functions in primary cultured astrocytes. To examine the role of TRPC channels in S1P-induced astrocytic responses, we examined Ca^{2+} responses, morphological changes, migration, and cytokine release. Here, we provide the first indication of the possibility that TRPC6 channels are involved in S1P-induced Ca^{2+} responses and CXCL1 release.

Materials and Methods

Cultured rat cortical astrocyte

All experiments were conducted in accordance with the ethical guidelines of the Kyoto University Animal Research Committee. Primary astrocyte-enriched cultures were prepared from cerebral cortices of 0–2 d-old postnatal Wistar/ST rats (Japan SLC, Hamamatsu, Japan), as previously described [Shirakawa et al., 2010] with slight modification. Cells were dissociated with 3 mg/ml dispase (Gibco, Tokyo, Japan), and were plated in 75 cm^2 bent-cap flasks with 7 ml of Eagle's Minimum Essential Medium (EMEM; Nissui Pharmaceutical, Tokyo, Japan) containing 10% heat-inactivated fetal bovine serum (FBS; JRH Biosciences, Lenexa, USA) in an incubator with 5% CO_2 at 37°C. After cultivation for 2–4 weeks, the flasks were shaken on an orbital shaker at 250 rpm for 14–17 h at 37°C to remove microglia and oligodendrocytes. The remaining astrocytes were detached with 0.25% trypsin (Gibco), resuspended in fresh medium, and reseeded on 10 mm glass coverslips, 35 mm dishes or 48 well plates at a density of 2.5×10^4 cells/cm^2. Cells were used at least 4-5 days before being used for experiments. Unless otherwise noted, all experiments were performed under serum starvation.

Reverse transcription (RT)-PCR

Total RNA was extracted from astrocytes in a 35 mm dish using a Nucleo Spin® RNA kit (TaKaRa Bio, Shiga, Japan). Using 1 μg of total RNA, two-step reverse transcription (RT)-PCR was performed with the ReverTra Ace® RT-PCR Kit (Toyobo, Osaka, Japan) using a PCR Thermal Cycler Dice® Gradient (Takara Bio; TP600). The pairs of primers used for

amplification were 5'-GAAGTTCCACCGGCCCATGT-3' and 5'-GGAGATGTTCTTGCGGAAGG-3' for S1P receptor 1 ($S1P_1$), 5'-GTCTGGACCATCTGGAGGCT-3' and 5'-GTCTGAGGACCAGCAACGTC-3' for S1P receptor 2 ($S1P_2$), 5'-GACGCCAACAAGAAGCACCG-3' and 5'-GCTGATGAGAAAGGCAATGTA-3' for S1P receptor 3 ($S1P_3$), 5'-TGGGGTGCCCAGAGGAGTCG-3' and 5'-CTAGCCAGCCTGCCGCTGTG-3' for S1P receptor 4 ($S1P_4$), 5'-GCCTATGTGCTCTTCTGCGT-3' and 5'-CAACGACCGTGGCGTGTG-3' for S1P receptor 5 ($S1P_5$), 5’-AAGAACTGCAGTCCTTCGTTG-3’ and 5’-TCTGCATCTTCTGTCGCATG-3’ for TRPC1, 5’-TCTGTTGTCCTCAAATATGACCAC-3’ and 5’-TCTCGAGTTAGACTGAGTGAAGAG-3’ for TRPC3, 5’-CTGGTCAAGTGGATATGGACG-3’ and 5’-CTTCGCTGTGGCTCTTCTC-3’ for TRPC4, 5’-TGGTTCAACAACACCTTCTGTC-3’ and 5’-ACCATTAAACTTGGAGAACAGGAG-3’ for TRPC5, 5‘-CGGATGTGGAGTGGAAGTTTG-3’ and 5’-CATAACGGAGACTTGAGATGTCC-3’ for TRPC6, and 5’-TGAAGTACGACCACAAGTTCATC-3’ and 5’-GCACGTATCTCTTAATGAGACGC-3’ for TRPC7. The temperature cycles were 94°C for 2 min, followed by 35 cycles of 94°C for 30 s, 58°C for 30 s, and 72°C for 45 s. Amplified PCR products were electrophoresed in a 1.2% TAE agarose gel and visualized under UV light with 0.1 μg/ml ethidium bromide by using a ChemiDoc XRS (Bio-Rad, Hercules, CA, USA). Images were captured with Quantity One software (Bio-Rad).

Measurement of intracellular Ca^{2+} concentrations

Intracellular Ca^{2+} concentration ($[Ca^{2+}]_i$) was monitored using the fluorescent calcium indicator fura 2-AM (Dojindo, Kumamoto, Japan), as previously described [Miyake et al., 2015]. Astrocytes were cultured on 10 mm glass coverslips and grown for 4–5 d. For dye loading, the cells on a coverslip were loaded for 30 min with 5 μM fura 2-AM in Krebs-Ringer solution (140 mM NaCl, 5 mM KCl, 1 mM $MgCl_2$, 2 mM $CaCl_2$, 10 mM glucose, 10 mM HEPES) containing 0.01% cremophor EL (Sigma-Aldrich). Cells were washed with Krebs-Ringer solution and set on an imaging chamber. For the Ca^{2+} -free experiments, $CaCl_2$ was omitted, and 0.5 mM EGTA was added to the external solution. Loaded cells were transferred into a perfusion chamber with fresh buffer and mounted on a Nikon fluorescent microscope equipped with an AQUACOSMOS/ORCA-AG imaging system (Hamamatsu Photonics, Shizuoka, Japan). Fluorescent images were scanned at 500 nm and 2 sec intervals, with alternate excitation at 340 and 380 nm at room temperature. The fluorescence ratio of individual cells is designated F340/380. Each experiment was repeated more than three times.

Quantitative RT-PCR

After RT of total mRNA to cDNA using ReverTra Ace® qPCR RT Master Mix (Toyobo), real-time quantitative PCR was performed using the StepOne real-time PCR system (Applied Biosystems, Darmstadt, Germany) in a final volume of 20 μl containing 0.5 μg of total RNA with THUNDERBIRD SYBR qPCR Mix (Toyobo). The oligonucleotide primers used for 18S ribosomal RNA (rRNA) were 5’-CGGTCCAAGAATTTCACCTC-3’ and 5’-ACCGCGGTTCTATTTTGTTG-3’, for BDNF were 5’-GAAGGCTGCAGGGGCATAGAC-3’ and 5’-TACACAGGAAGTGTCTATCCTTAT-3’, for

GDNF were 5’-CTCGAAGAGAGAGGAACCGGCAAG-3’ and 5’-CTGGAGCCAGGGTCAGATACATCC-3’, for NGF were 5’-CAGAGTTTTGGCCTGTGGT-3’ and 5’-GGACATTACGCTATGCACCTC-3’, for COX-2 were 5’-GATCACATTTGATTGACAGC-3’ and 5’-TCCTTATTTCCTTTCACACC-3’, for ICAM1 were 5’-TATCGGGATGGTGAAGTCTG-3’ and 5’-ATTCTGATCATGGTACAGCAC-3’, for IL6 were 5’-ACTTCACAGAGGATACCAC-3’ and 5’-GCATCATCGCTGTTCATAC-3’, for CCL5 were 5’-CCAGAGAAGAAGTGGGTTCA-3’ and 5’-AGCAAGCAATGACAGGAAAG-3’, for CXCL10 were 5’-TGAAAGCGGTGAGCCAAAGA-3’ and 5’-TAGCCGCACACTGGGTAAAG-3’, for CXCL1 were 5’-CAGCGCTGCACAGAGAAG-3’ and 5’-GACTCCAGCCACACTCCAA-3’ and TRPC6 were 5-‘AGGAAATTGAGGATGATGCGG-3’ AND 5’-CCCTGGATAAGCTCAGACATCC-3’. The temperature cycles were 95°C for 10 min, followed by 35 cycles of 95°C for 15 s and 60°C for 60 s. The results were analyzed with Primer Express software (Applied Biosystems). The identity of the PCR product was confirmed by automated determination of the melting temperature of the PCR products. The results for each gene were normalized to 18S rRNA levels measured in parallel in each sample.

Measurement of CXCL1

CXCL1 release or content was measured using a rat CXCL1/CINC-1 Quantikine ELISA Kit (R&D Systems, Minneapolis, MN) according to the manufacturer’s instructions. For the assay, cells were grown in 48 well plates for at least 1 week. After serum starved overnight, cells were

treated with S1P or vehicle control for 48 h in the absence or presence of each inhibitor. After the treatments, 50 μL of culture supernatant was analyzed.

Western blotting

Western blotting was performed as described previously [Shirakawa et al., 2010], with slight modification. The drugs-treated cells were collected by a brief centrifugation and were lysed in RIPA buffer (Nacalai tesque, Kyoto, Japan) supplemented with phosphatase inhibitor cocktail 2 and 3 (P5726 and P0044, Sigma Aldrich). Proteins were diluted in NuPAGE® 4x LDS sample buffer (Life Technologies, Carlsbad CA, USA), loaded onto a 10% SDS-polyacrylamide gel, and blotted onto Immobilon-P PVDF transfer membranes (Millipore, Bedford, MA, USA). After a blocking step using Blocking One-P (Nacalai tesque), the membranes were incubated overnight at 4°C with primary antibodies, which were all purchased from Cell Signaling Technologies, (Beverly, MA, USA) diluted 1:1000 in Tris-buffered saline containing 0.1% Tween-20 and 10% Blocking One-P. Phosphorylated proteins were detected using rabbit monoclonal or polyclonal antibodies against phospho-p44/42 MAPK (Erk1/2) (#9101), phospho-SAPK/JNK (#4671) and phospho-p38 MAPK (#9211) followed by incubation with peroxidase-conjugated donkey anti-rabbit IgG (1:5000 dilution; GE Healthcare, Little Chalfont, UK) for 1 h at RT. Specific bands were detected by Immobilon Western Chemiluminescent HRP substrate (Millipore) and visualized using the ChemiImager 4400 imaging system (Alpha Innotech, San Leandro, CA, USA). To normalize for total protein loading, blots were stripped and reprobed with rabbit polyclonal antibodies against SAPK/JNK (#9252), p44/42 MAPK (Erk1/2) (#9102), or p38 MAPK (#9212) followed by the same procedure as described above.

The bands were densitometrically quantified using ImageJ software.

TRPC6 siRNA transfection

TRPC6-specific siRNA was used to block TRPC6-mediated signaling. Astrocytes were transfected with Stealth™ RNAi Negative Control Medium GC Duplex or Stealth™ select RNAi for rat TRPC6 (Life Technologies) using Lipofectamine 2000 transfection reagent (Life Technologies) according to the manufacturer's instructions. The Stealth™ select RNAi sequence for rat TRPC6 was 5'-UUCAAUAGGAGAUAAAGCAGGGACU-3' and 5'-AGUCCCUGCUUUAUCUCCUAUUGAA. After 6 h of treatment with siRNA, the medium was replaced and the cells were incubated for 48 h. The transfection rate was calculated to be ≥90%, as estimated by the percentage of cells that were fluorescein isothiocyanate-positive after being treated with Block-iT Fluorescent Oligo dsRNA (Life Technologies) as a transfection control.

Fluorescence staining

S1P-induced morphological changes were detected by actin staining, as previously described [Shirakawa et al., 2010; Miyanohara et al., 2015]. After pre-treatment with serum-free EMEM for 10 min, cells on 10 mm glass coverslips (Matsunami Glass, Osaka, Japan) were treated with the drug of interest for 3 h. Following fixation with 4% para-formaldehyde, the cells were soaked in 0.2% Tri-ton-X100 for permeabilization, and then incubated for 1 h at 4°C with rabbit Alexa Fluor488-conjugated phalloidin (1:40 dilution; Invitrogen, Carlsbad, CA, USA) to visualize the actin cytoskeleton. Before observation with a fluorescence microscope, 0.01

mg/ml Hoechst 33342 was added to the cells on the glass for nuclear staining. Astrocyte were defined as “polygonal cells” in the morphology if they exhibit polygonal shapes with an increase in their F-actin content adjacent to the cell membrane and do not display multipolar shapes with diffuse F-actin extending short protrusions, which were commonly observed in control treatment under serum starvation. Morphological changes were calculated as the percentage of polygonal-shaped astrocytes to the total number of Hoechst-positive cells.

Scratch-wound assay

After enrichment of the cortical astrocytes, the cells were reseeded on 35 mm dishes and cultured for 1–2 weeks. Following serum starvation for 24 h, the medium was removed, and a reference line was drawn. A scratch was made in the astrocyte monolayer with a 1 ml pipette tip along the reference line, creating 4–8 scratched areas. Cells were washed twice with phosphate-buffered saline to remove cell debris, and fresh serum-free media containing the drugs of interest were added. Images were taken at 0 and 72 h, with the same field recorded in each case. To determine the area of migration, the leading edge of the scratched cells at 0 h was superimposed onto the image taken at 72 h. After treatments, measurements from 4–8 areas were averaged to determine the area of migration.

Statistical analysis

Data were expressed as means ± S.E.M. The statistical significance of the differences among groups was determined by a one-way analysis of variance (ANOVA) followed by Tukey’s multiple comparison tests using GraphPad Prism 5 (GraphPad Software, La Jolla, CA, USA)

and a p-value of less than 5% was considered significant.

Results

S1P receptors $S1P_1$, $S1P_2$, and $S1P_3$ are expressed in primary rat cortical astrocytes

S1P receptors are a family of G protein-coupled receptors (GPCRs), consisting of five members called $S1P_1$, $S1P_2$, $S1P_3$, $S1P_4$, and $S1P_5$ [Brinkmann, 2007; Pyne and Pyne, 2010]. First, we investigated the expression of the S1P receptor subtypes in cultured rat primary cortical astrocytes. RT-PCR analysis of mRNA extracted from cultured astrocytes detected the expression of $S1P_1$, $S1P_2$, and $S1P_3$ but not $S1P_4$ and $S1P_5$ (Fig. 1A).

S1P induces Ca^{2+} mobilization in cultured cortical astrocytes via G_q-coupled receptors $S1P_2$ and $S1P_3$

S1P stimulates the $G_{q/11}$-inositol lipid/Ca^{2+} signaling pathway in cortical astrocytes [Sorensen et al., 2003]. To investigate S1P-induced Ca^{2+} responses, $[Ca^{2+}]_i$ was measured by Ca^{2+} imaging experiments using fura-2 AM, with the finding that S1P evoked Ca^{2+} responses in a concentration-dependent manner and that the responses consisted of a large and transient increase in $[Ca^{2+}]_i$, followed by a sustained increase (Fig. 1B-E). We assessed the Ca^{2+} responses by quantifying the transient increase in $[Ca^{2+}]_i$ resulting from Ca^{2+} release from the endoplasmic reticulum (ER), called the “peak amplitude”, and the persistent increase in $[Ca^{2+}]_i$ resulting from Ca^{2+} entry as the “sustained level”.

To investigate which S1P receptor subtypes are responsible for S1P-induced Ca^{2+} mobilization, we examined whether $S1P_1$ stimulation can evoke Ca^{2+} responses and found that a selective $S1P_1$ agonist SEW2871 (10 μM) did not evoke Ca^{2+} responses (Fig. 1F). Next, we examined whether Ca^{2+} responses are suppressed by either an inhibitor of G_q-coupled receptor

$S1P_2$ or $S1P_3$. A selective $S1P_2$ inhibitor JTE013 (1 μM) significantly but partially suppressed both the peak amplitude and the sustained increase of $[Ca^{2+}]_i$ (Fig. 1G), and a selective $S1P_3$ inhibitor CAY10444 (10 μM) had a tendency to suppress peak amplitude and significantly but partially suppressed the sustained Ca^{2+} response (Fig. 1H). In addition, PLC inhibitor U73122 (1 μM) completely inhibited the S1P-induced Ca^{2+} elevation (Fig. 1I), while the $G_{\beta\gamma}$ subunit activity inhibitor gallein (10 μM) had no effect on the Ca^{2+} responses (Fig. 1J), suggesting that G_q protein, but not $G_{\beta\gamma}$, is involved in these observed Ca^{2+} responses. Taken together, these results suggest that S1P induces Ca^{2+} responses via the G_q-coupled receptors $S1P_2$ and $S1P_3$.

S1P-induced Ca^{2+} responses can be attributed to TRPC-mediated extracellular Ca^{2+} entry in cultured astrocytes

We investigated the contribution of extracellular Ca^{2+} to the S1P-induced response in astrocytes. Under Ca^{2+}-free conditions, only transient Ca^{2+} elevation, without subsequent sustained increases in $[Ca^{2+}]_i$, was observed (Fig. 2A), suggesting that the sustained increase in $[Ca^{2+}]_i$ was dependent on the extracellular Ca^{2+} level. In addition, we examined the involvement of the TRP channels, which are Ca^{2+}-permeable cation channels, using non-selective TRP channel inhibitors Gd^{3+} (10 μM) and La^{3+} (10 μM). Gd^{3+} and La^{3+} significantly suppressed the sustained Ca^{2+} responses, but not the peak amplitude (Fig. 2B, C).

TRPC channels are activated by diacylglycerol activation [Birnbaumer, 2009], which occurs after G_q-coupled receptor stimulation and contributes to Ca^{2+} responses in astrocytes [Grimardi, 2006]. We investigated the expression of TRPC channels by RT-PCR analysis and detected specific high-intensity bands for TRPC1, C4, and C6 and a relatively low-intensity band for

TRPC3 and C5 (Fig. 2D). We investigated the involvement of TRPC channels in S1P-induced Ca^{2+} responses. Application of the non-selective TRPC inhibitor Pyr2 significantly inhibited the peak amplitude and sustained increase in $[Ca^{2+}]_i$ (Fig. 2E). On the other hand, the selective TRPC3 inhibitor Pyr3 did not affect the S1P-induced sustained increase in $[Ca^{2+}]_i$, while it significantly, albeit weakly, suppressed the peak amplitude (Fig. 2F), indicating that TRPC6 is involved in both S1P-induced peak amplitude and sustained increase in $[Ca^{2+}]_i$.

S1P-induced morphological change is independent of Ca^{2+} signaling mediated by TRPC channels

S1P rearranges the actin cytoskeleton, leading to changes in astrocytic morphology [Rouach et al., 2006]. Staining with fluorescence-conjugated phalloidin revealed that continuous application of S1P (1 μM) for 3 h caused actin cytoskeletal rearrangements and retraction of the protrusions in serum-starved astrocytes, most of which exhibited a typical polygonal shape (Fig. 3). BAPTA-AM (3 μM), Pyr2 (10 μM), and Pyr3 (10 μM) all failed to inhibit this S1P-induced actin rearrangement with a polygonal morphology and cells treated with these reagents looked similar to those exposed to S1P (Fig. 3), indicating that S1P-induced morphological change is independent of TRPC activation in astrocytes.

S1P-induced astrocytic migration is independent of TRPC channel-mediated Ca^{2+} signaling

S1P promotes cellular migration in rat cortical astrocytes [Mullershausen, 2007]. Next, using a scratch-wound assay on a monolayer of pure astrocytes, we examined the effects of Pyr2 or Pyr3 on astrocytic migration and found that S1P significantly increased astrocytic migration and

that neither Pyr2 (10 μM) nor Pyr3 (10 μM) affects S1P-induced astrocytic migration (Fig. 4), suggesting that S1P-induced migration is independent of TRPC activation in astrocytes.

S1P increases CXCL1 expression and release from astrocytes via G_q-coupled receptors $S1P_2$ and $S1P_3$

Physiologically or abnormally activated astrocytes may produce and release some cytokines, inflammatory factors, and neurotrophic factors [Allaman et al., 2011; Verkhratsky, 2016]. Additionally, S1P-treated astrocytes release GDNF [Yamagata et al., 2003], NGF [Furukawa et al., 2007], Il1β, and CCL2 [Zhou et al., 2004]. Therefore, we investigated changes in the expression level of various factors 24 h after treatment with 1 μM S1P. Among tested genes, we found that the mRNA for only CXCL1, one of the CXC chemokines, was significantly upregulated in S1P-treated astrocytes (Fig. 5A-H). Using ELISA assay, we measured the content of CXCL1 in the culture medium of astrocytes treated with S1P (1 μM) after 24 h and found that S1P increased the CXCL1 release, which was significantly inhibited by the $S1P_2$ receptor inhibitor JTE013 at 1 μM and the $S1P_3$ receptor inhibitor CAY10444 at 10 μM, but not the $S1P_1$ receptor inhibitor VPC44116 at 1 μM (Fig. 5I). These findings indicate that S1P increased CXCL1 production and release via G_q-coupled receptors $S1P_2$ and $S1P_3$ in astrocytes (Fig. 5I).

S1P-induced CXCL1 release is mediated by TRPC6, Ca^{2+} signaling, and the MAPK pathway

Finally, we investigated the mechanisms underlying S1P-induced CXCL1 release. Mitogen-activated protein kinases (MAPKs), a family of serine/threonine kinases, link receptor activation in the cell membrane to gene expression in the nucleus [Chang and Karin, 2001]. We

examined the phosphorylation levels of MAPKs, such as ERK, JNK and p38, in the presence and absence of S1P and found that phosphorylation levels of all MAPKs significantly increased in S1P-stimulated astrocytes (Fig. 6A). Moreover, S1P-induced CXCL1 release was significantly inhibited by MEK inhibitor PD98059 (30 μM), JNK inhibitor SP600125 (SP) (30 μM), or p38 inhibitor SB203580 (SB) (30 μM) (Fig. 6B). The non-selective TRPC channel inhibitor Pyr2 (1–10 μM), but not the selective TRPC3 inhibitor Pyr3, significantly inhibited the increase in CXCL1 release (Fig. 6C, D). To determine whether the Ca^{2+} signal may participate in CXCL1 release, we used the PKC inhibitor bisindolylmaleimide I (BIM; 1 μM), ER Ca^{2+}-ATPase inhibitor cyclopiazonic acid (CPA; 30 μM), and intracellular Ca^{2+} chelator BAPTA-AM (3 μM) and found that all the drugs significantly blocked S1P-induced CXCL1 release (Fig. 6E). Collectively, these results suggest that S1P induces Ca^{2+} entry through TRPC channels, which could activate MAPK signaling and result in an increase in CXCL1 release.

Among the TRPC channels, TRPC1, 4, and 6 were abundantly expressed in our astrocyte preparation, and, since TRPC1 and TRPC4 themselves do not form a functional channel [Birnbaumer, 2009; Kiyonaka et al., 2009]. We focused on the role of TRPC6 in mediating S1P-induced CXCL1 release. We developed a specific siRNA for TRPC6 (si-TRPC6) and found that it reduced the mRNA levels of TRPC6 by more than 50% (Fig. 6F). Subsequently, we confirmed selective TRPC6 knockdown using the DAG analogue OAG, which is a direct activator of TRPC3, 6, and 7. The percentage of cultured astrocytes responding to OAG was also significantly reduced by si-TRPC6 treatment (Fig. 6G-I), indicating that TRPC6 function was partially and significantly suppressed with si-TRPC6 treatment. On the other hand, treatment with OAG at ranging from 1 to100 μM did not induce CXCL1 release (Fig. 6J),

suggesting that OAG alone can induce astrocytic Ca^{2+} responses, but does not mimic S1P-induced CXCL1 release. Moreover, we examined the response to S1P in TRPC6 down-regulated astrocytes and found that S1P-induced sustained increase, but not the peak amplitude, in $[Ca^{2+}]_i$ was significantly inhibited by down-regulation of TRPC6 with si-TRPC6 (Fig. 3K-N). Subsequently, we examined the effects of RNAi-mediated knockdown of TRPC6 on CXCL1 release. After 24 h of treatment with S1P, si-TRPC6 significantly inhibited S1P-induced CXCL1 release (Fig. 6O), demonstrating that TRPC6 contributes to S1P-induced Ca^{2+} responses and CXCL1 release.

Discussion

In this study, we investigated S1P-induced Ca^{2+} responses and CXCL1 release and found that S1P induced stimulation of G_q-coupled receptors $S1P_2$ and $S1P_3$ following Ca^{2+} influx via TRPC6, which resulted in activation of the MAPK pathway and CXCL1 release.

Ca^{2+} signaling via TRPC6 was involved in S1P-induced Ca^{2+} responses and CXCL1 release but not in morphological changes and migration. The reason for this difference is unclear. Since S1P induces morphological change via $G_{12/13}$ and the Rho pathway, proliferation via $G_{i/o}$, [Sorensen et al., 2003], and migration via $S1P_1$ [Mullershausen et al., 2007], Ca^{2+} signaling may not be important in these cellular responses. On the other hand, we previously reported that a thrombin receptor proteinase-activated receptor 1 (PAR1), coupled with $G_{q/11}$, $G_{12/13}$, and $G_{i/o}$, induces proliferation and morphological changes that are mediated by Ca^{2+} signaling via TRPC3 [Shirakawa et al., 2010]. Therefore, whether Ca^{2+} signaling is involved in cellular function may depend on the coupled G protein. S1P evoked a transient Ca^{2+} peak followed by sustained elevation of $[Ca^{2+}]_i$, although thrombin induces a transient Ca^{2+} response followed by Ca^{2+} oscillation. This different Ca^{2+} signaling pattern may be attributed to the differences in downstream Ca^{2+}-binding proteins or signals. In this study, we demonstrated that TRPC6 is involved in S1P-induced responses, but the role of TRPC6 in astrocytes was reported in only one study in the literature, which reported increases in TRPC6 expression after IL1β treatment that involved OAG-induced Ca^{2+} responses [Beskina et al., 2007]. Future studies are needed to determine the detailed molecular pathways that TRPC6-mediated Ca^{2+} signaling may regulate in astrocytes.

One could question whether S1P-induced TRPC6-mediated Ca^{2+} signaling can regulate the activation of MAPKs pathway. Consistent with the observation in this study, Osinde et al. (2007) reported that S1P stimulates ERK phosphorylation via $S1P_3$, but not $S1P_1$ receptors, in cultured astrocyte. On the other hand, Sorensen et al. (2003) reported that S1P-induced ERK and JNK phosphorylation are dependent on pertussis toxin-sensitive $G_{i/o}$ proteins, implying that Ca^{2+} signaling is not always necessary to activate MAPK. In this context, Miyabe et al. (2016) have reported that S1P at 5 μM induces CXCL1 release in human umbilical vein endothelial cells, which is significantly inhibited by a functional $S1P_1$ antagonist ONO-W061. These studies suggest the involvement of TRPC6-mediated Ca^{2+} signaling in S1P-induced MAPKs activation and CXCL1 release is partial and there could be other independent parallel pathways.

Sphingosine kinase, which can phosphorylate sphingosine to produce S1P, is highly expressed in the brain [Fukuda et al., 2003], and the S1P receptors ($S1P_{1-5}$) that belong to the GPCR super family are also expressed in brain cells, including astrocytes [Groves et al., 2013]. There have been some reports indicating that S1P induces the expression of some neurotrophic factors including GDNF [Yamagata et al., 2003] and NGF [Furukawa et al., 2007] in cultured astrocytes, which were not consistent with our observations that rat cultured rat astrocytes did not show any change in GDNF and NGF mRNA levels by S1P treatment for 24 h. Since the previous studies demonstrate that S1P-induced increase in the mRNA expression levels of NGF as well as GDNF can peak at 6-12 h, gradually decline to control level by 24 h, further time-course study will be needed to address the discrepancy in the responses to S1P.

Conversely, S1P can be involved in neuroinflammatory diseases in various pathological conditions. For example, the concentration of S1P in the brain increases after ischemia in a

mouse thrombosis model of the middle cerebral artery [Kimura et al., 2008], and S1P production is facilitated in reactive astrocytes and activated microglia [Kimura et al., 2007]. Also, in the cerebrospinal fluid of multiple sclerosis (MS) patients, the S1P concentration [Kułakowska et al., 2010] and $S1P_1$ and $S1P_3$ are upregulated in MS lesions [Van Doorn, 2010]. Since S1P concentrations are high in blood but low in tissues [Obinata and Hla, 2012], S1P can leak and affect the CNS environment when the blood-brain barrier becomes permeable in some pathological conditions.

In this study, S1P promoted CXCL1 release after G_q-coupled receptor stimulation. Stimulation of other G_q-coupled receptors results in an increase in CXCL1 production or secretion. For example, thrombin or agonist of PAR1 induced CXCL1 release from astrocytes via Ca^{2+} signaling [Wang et al., 2007]. Activation of endothelin B receptor also promotes CXCL1 production mediated by the NF-κB pathway [Koyama et al., 2013]. Although CXCL1 can exacerbate inflammation by promoting neutrophil migration in neuroinflammatory diseases, CXCL1 production was induced by pro-inflammatory factors, such as LPS [McKimmie and Graham, 2010], TNFα [Lee et al., 2012], and IL1β [An et al., 2011], in astrocytes. Treatment with a neutralizing antibody for CXCL1 or an antagonist for CXCR1/2, a receptor of CXCL1, improves neurological symptoms in murine models of inflammatory pain [Cao et al., 2014], cerebral ischemia [Garau et al., 2006], spinal cord injury [Gorio et al., 2007], and cerebral hemorrhage [Matsushita et al., 2014]. Since S1P is upregulated in these diseases [Obinata and Hla, 2012], so it is conceivable that an increase in CXCL1 production in astrocytes is involved in exacerbation of inflammation in these neuroinflammatory diseases.

Meanwhile, CXCL1 also has beneficial effects by promoting oligodendrocyte progenitor proliferation [Wu et al., 2000], and controlling positioning of oligodendrocyte precursors [Tsai et al., 2002]. In MS mouse models, studies report conflicting results showing that CXCL1 is either proinflammatory or neuroprotective [Omari et al., 2006]. Therefore, whether CXCL1 from astrocytes promotes neuroinflammation or has a beneficial effect may depend on each pathological condition and disease stage.

In conclusion, this study demonstrated that S1P induces Ca^{2+} influxes via TRPC6, which activates the MAPK pathway to promote CXCL1 release. Since S1P is upregulated in inflammatory diseases, S1P-induced CXCL1 release may be important in inhibiting CNS inflammation, in which excessive astrocytic activation plays a role.

Acknowledgements

This study was supported by a Grant-in-aid for Scientific Research from the Ministry of Education, Culture, Sports, Science, and Technology, Japan, and from the Japan Society for the Promotion of Science. This work was also supported by the Research Foundation for Pharmaceutical Sciences, the Naito Foundation and the Takeda Science Foundation. The authors declare no competing financial interests.

Reference

Allaman I, Bélanger M, Magistretti PJ. 2011. Astrocyte-neuron metabolic relationships: for better and for worse. Trends Neurosci 34:76-87.

An Y, Chen Q, Quan N. 2011. Interleukin-1 exerts distinct actions on different cell types of the brain in vitro. J Inflamm Res 2011:11-20.

Bazargani N, Attwell D. 2016. Astrocyte calcium signaling: the third wave. Nat Neurosci. 19:182-189.

Beskina O, Miller A, Mazzocco-Spezzia A, Pulina MV, Golovina VA. 2007. Mechanisms of interleukin-1beta-induced Ca^{2+} signals in mouse cortical astrocytes: roles of store- and receptor-operated Ca^{2+} entry. Am J Physiol Cell Physiol 293:C1103-1111.

Birnbaumer L. 2009. The TRPC class of ion channels: a critical review of their roles in slow, sustained increases in intracellular Ca(2+) concentrations. Annu Rev Pharmacol Toxicol. 49:395-426.

Brinkmann V. 2007. Sphingosine 1-phosphate receptors in health and disease: mechanistic insights from gene deletion studies and reverse pharmacology. Pharmacol Ther 115:84-105.

Cao DL, Zhang ZJ, Xie RG, Jiang BC, Ji RR, Gao YJ. 2014. Chemokine CXCL1 enhances inflammatory pain and increases NMDA receptor activity and COX-2 expression in spinal cord neurons via activation of CXCR2. Exp Neurol 261:328-336.

Chang L, Karin M. 2001. Mammalian MAP kinase signalling cascades. Nature 410:37-40.

Fiacco TA, McCarthy KD. 2006. Astrocyte calcium elevations: properties, propagation, and effects on brain signaling. Glia 54:676-690.

Fischer I, Alliod C, Martinier N, Newcombe J, Brana C, Pouly S. 2011. Sphingosine kinase 1 and sphingosine 1-phosphate receptor 3 are functionally upregulated on astrocytes under pro-inflammatory conditions. PLoS One 6:23905.

Fukuda Y, Kihara A, Igarashi Y. 2003. Distribution of sphingosine kinase activity in mouse tissues: contribution of SPHK1. Biochem Biophys Res Commun 309:155-160.

Furukawa A, Kita K, Toyomoto M, Fujii S, Inoue S, Hayashi K, Ikeda K. 2007. Production of nerve growth factor enhanced in cultured mouse astrocytes by glycerophospholipids, sphingolipids, and their related compounds. Mol Cell Biochem 305:27-34.

Garau A, Bertini R, Mosca M, Bizzarri C, Anacardio R, Triulzi S, Allegretti M, Ghezzi P, Villa P. 2006. Development of a systemically-active dual CXCR1/CXCR2 allosteric inhibitor and its efficacy in a model of transient cerebral ischemia in the rat. Eur Cytokine Netw 17:35-41.

Golovina VA. 2005. Visualization of localized store-operated calcium entry in mouse astrocytes. Close proximity to the endoplasmic reticulum. J Physiol 564:737-749.

Gorio A, Madaschi L, Zadra G, Marfia G, Cavalieri B, Bertini R, Di Giulio AM. 2007. Reparixin, an inhibitor of CXCR2 function, attenuates inflammatory responses and promotes recovery of function after traumatic lesion to the spinal cord. J Pharmacol Exp Ther 322:973-981.

Grimaldi M. 2006. Astrocytes refill intracellular Ca^{2+} stores in the absence of cytoplasmic [Ca^{2+}] elevation: a functional rather than a structural ability. J Neurosci Res 84:1738-1749.

Groves A, Kihara Y, Chun J. 2013. Fingolimod: direct CNS effects of sphingosine 1-phosphate (S1P) receptor modulation and implications in multiple sclerosis therapy. J Neurol Sci 328:9-18.

Khakh BS, Sofroniew MV. 2015. Diversity of astrocyte functions and phenotypes in neural circuits. Nat Neurosci 18:942-952.

Kimura A, Ohmori T, Kashiwakura Y, Ohkawa R, Madoiwa S, Mimuro J, Shimazaki K, Hoshino Y, Yatomi Y, Sakata Y. 2008. Antagonism of sphingosine 1-phosphate receptor-2 enhances migration of neural progenitor cells toward an area of brain. Stroke 39:3411-3417.

Kimura A, Ohmori T, Ohkawa R, Madoiwa S, Mimuro J, Murakami T, Kobayashi E, Hoshino Y, Yatomi Y, Sakata Y. 2007. Essential roles of sphingosine 1-phosphate/$S1P_1$ receptor axis in the migration of neural stem cells toward a site of spinal cord injury. Stem Cells 25:115-124.

Kiyonaka S, Kato K, Nishida M, Mio K, Numaga T, Sawaguchi Y, Yoshida T, Wakamori M, Mori E, Numata T, Ishii M, Takemoto H, Ojida A, Watanabe K, Uemura A, Kurose H, Morii T, Kobayashi T, Sato Y, Sato C, Hamachi I, Mori Y. 2009. Selective and direct inhibition of TRPC3 channels underlies biological activities of a pyrazole compound. Proc Natl Acad Sci U S A 106:5400-5405.

Koyama Y, Kotani M, Sawamura T, Kuribayashi M, Konishi R, Michinaga S. 2013. Different actions of endothelin-1 on chemokine production in rat cultured astrocytes: reduction of CX3CL1/fractalkine and an increase in CCL2/MCP-1 and CXCL1/CINC-1. J Neuroinflammation 10:51.

Kułakowska A, Zendzian-Piotrowska M, Baranowski M, Konończuk T, Drozdowski W, Górski J, Bucki R. 2010. Intrathecal increase of sphingosine 1-phosphate at early stage multiple sclerosis. Neurosci Lett 477:149-152.

Lee YH, Kim SH, Kim Y, Lim Y, Ha K, Shin SY. 2012. Inhibitory effect of the antidepressant imipramine on NF-κB-dependent CXCL1 expression in TNFα-exposed astrocytes. Int Immunopharmacol 12:547-555.

Malchinkhuu E, Sato K, Muraki T, Ishikawa K, Kuwabara A, Okajima F. 2003. Assessment of the role of sphingosine 1-phosphate and its receptors in high-density lipoprotein-induced stimulation of astroglial cell function. Biochem J 15:817-827.

Matsushita H, Hijioka M, Ishibashi H, Anan J, Kurauchi Y, Hisatsune A, Seki T, Shudo K, Katsuki H. 2014. Suppression of CXCL2 upregulation underlies the therapeutic effect of the retinoid Am80 on intracerebral hemorrhage in mice. J Neurosci Res 92:1024-1034.

McKimmie CS, Graham GJ. 2010. Astrocytes modulate the chemokine network in a pathogen-specific manner. Biochem Biophys Res Commun 394:1006-1011.

Miyabe C, Miyabe Y, Komiya T, Shioya H, Miura NN, Takahashi K, Ohno N, Tsuboi R, Luster AD, Kawai S, Miyasaka N, Nanki T. 2016. A sphingosine 1-phosphate receptor agonist ameliorates animal model of vasculitis. Inflamm Res, *in press*.

Miyake T, Shirakawa H, Nakagawa T, Kaneko S. 2015. Activation of mitochondrial transient receptor potential vanilloid 1 channel contributes to microglial migration. Glia 63:1870-1872.

Miyanohara J, Shirakawa H, Sanpei K, Nakagawa T, Kaneko S. 2015. A pathophysiological role of TRPV1 in ischemic injury after transient focal cerebral ischemia in mice. Biochem Biophys Res Commun 467:478-483.

Mullershausen F, Craveiro LM, Shin Y, Cortes-Cros M, Bassilana F, Osinde M, Wishart WL, Guerini D, Thallmair M, Schwab ME, Sivasankaran R, Seuwen K, Dev KK. 2007.

Phosphorylated FTY720 promotes astrocyte migration through sphingosine-1-phosphate receptors. J Neurochem 102:1151-1161.

Mulligan SJ, MacVicar BA. 2004. Calcium transients in astrocyte endfeet cause cerebrovascular constrictions. Nature 431:195-199.

Obinata H, Hla T. 2012. Sphingosine 1-phosphate in coagulation and inflammation. Semin Immunopathol 2012 34:73-91.

Omari KM, John G, Lango R, Raine CS. 2006. Role for CXCR2 and CXCL1 on glia in multiple sclerosis. Glia 53:24-31.

Osinde M, Mullershausen F, Dev KK. 2007. Phosphorylated FTY720 stimulates ERK phosphorylation in astrocytes via S1P receptors. Neuropharmacology 52:1210-1218.

Pyne NJ, Pyne S. 2010. Sphingosine 1-phosphate and cancer. Nat Rev Cancer 10:489-503.

Rouach N, Pébay A, Même W, Cordier J, Ezan P, Etienne E, Giaume C, Tencé M. 2006. S1P inhibits gap junctions in astrocytes: involvement of G and Rho GTPase/ROCK. Eur J Neurosci 23:1453-1464.

Rusakov DA. 2015. Disentangling calcium-driven astrocyte physiology. Nat Rev Neurosci 16:226-233.

Shirakawa H, Sakimoto S, Nakao K, Sugishita A, Konno M, Iida S, Kusano A, Hashimoto E, Nakagawa T, Kaneko S. 2010. Transient receptor potential canonical 3 mediates thrombin-induced astrocyte activation and upregulates its own expression in cortical astrocytes. J Neurosci 30:13116 -13129.

Sofroniew MV. 2009. Molecular dissection of reactive astrogliosis and glial scar formation. Trends Neurosci 32:638-647.

Sorensen SD, Nicole O, Peavy RD, Montoya LM, Lee CJ, Murphy TJ, Traynelis SF, Hepler JR. 2003. Common signaling pathways link activation of murine PAR-1, LPA, and S1P receptors to proliferation of astrocytes. Mol Pharmacol 64:1199-209.

Tsai HH, Frost E, To V, Robinson S, Ffrench-Constant C, Geertman R, Ransohoff RM, Miller RH. 2002. The chemokine receptor CXCR2 controls positioning of oligodendrocyte precursors in developing spinal cord by arresting their migration. Cell 110:373-383.

Van Doorn R, Van Horssen J, Verzijl D, Witte M, Ronken E, Van Het Hof B, Lakeman K, Dijkstra CD, Van Der Valk P, Reijerkerk A, Alewijnse AE, Peters SL, De Vries HE. 2010. Sphingosine 1-phosphate receptor 1 and 3 are upregulated in multiple sclerosis lesions. Glia. 58:1465-1476.

Verkhratsky A, Matteoli M, Parpura V, Mothet JP, Zorec R. 2016. Astrocytes as secretory cells of the central nervous system: idiosyncrasies of vesicular secretion. EMBO J 35:239-257.

Wang Y, Luo W, Reiser G. 2007. The role of calcium in protease-activated receptor-induced secretion of chemokine GRO/CINC-1 in rat brain astrocytes. J Neurochem 103:814-819.

Wu Q, Miller RH, Ransohoff RM, Robinson S, Bu J, Nishiyama A. 2000. Elevated levels of the chemokine GRO-1 correlate with elevated oligodendrocyte progenitor proliferation in the jimpy mutant. J Neurosci 20:2609-2617.

Yamagata K, Tagami M, Torii Y, Takenaga F, Tsumagari S, Itoh S, Yamori Y, Nara Y. 2003. Sphingosine 1-phosphate induces the production of glial cell line-derived neurotrophic factor and cellular proliferation in astrocytes. Glia 41:199-206.

Zhou H, Murthy KS. 2004. Distinctive G protein-dependent signaling in smooth muscle by sphingosine 1-phosphate receptors $S1P_1$ and $S1P_2$. Am J Physiol Cell Physiol 286:C1130-1138.

Figure legends

Fig. 1. Expression of S1P receptors and S1P-induced Ca^{2+} responses in primary rat cortical astrocytes.

(A) RT-PCR analysis for metabotropic S1P receptors by RT-PCR. Marker (M) shows the 100 bp DNA size ladder. (B-E) Ca^{2+} responses to S1P at the indicated concentrations (0.01–10 μM). (F) Intracellular Ca^{2+} level after treatment with the selective $S1P_1$ agonist SEW2871 (10 μM). (G-J) Representative traces and quantitative data of peak Ca^{2+} amplitude and sustained Ca^{2+} concentration due to S1P (1 μM)-induced Ca^{2+} mobilization after treatment with selective $S1P_2$ inhibitor JTE013 (1 μM) (G), selective $S1P_3$ inhibitor CAY10444 (10 μM) (H), PLC inhibitor U73122 (1 μM) (I), or $G_{\beta\gamma}$ subunit activity inhibitor gallein (10 μM) (J). $*P < 0.05$, $**P < 0.01$ vs. S1P alone (n = 6–16). Drugs were applied during the periods indicated by the horizontal lines.

Fig. 2. Involvement of TRPC channels in S1P-induced Ca^{2+} responses in cultured rat astrocytes.

(A) S1P-induced Ca^{2+} responses under extracellular Ca^{2+}-free conditions. (B, C) Representative traces and quantitative data of peak Ca^{2+} amplitude and sustained Ca^{2+} concentration due to S1P (1 μM)-induced Ca^{2+} mobilization after treatment with non-selective TRP inhibitor Gd^{3+} (10 μM) (B) or La^{3+} (10 μM) (C). (D) RT-PCR analysis of TRPC channels in primary rat cortical astrocytes. (E, F) Astrocytes were treated with non-selective TRPC inhibitor Pyr2 (10 μM) (E) or selective TRPC3 inhibitor Pyr3 (3 μM) (F). $*P < 0.05$, $**P < 0.01$ vs. S1P alone (n = 3–13).

Fig. 3. S1P-induced morphological changes in cultured rat astrocytes. Representative photographs were obtained from serum-starved rat cortical astrocytes that received control treatment (A), S1P at 1 μM (B), S1P and BAPTA-AM at 3 μM (C), S1P and Pyr2 at 10 μM (D), or S1P and Pyr3 at 10 μM (E) for 3 h. The actin cytoskeleton was detected by phalloidin staining, shown in green fluorescence. Cellular nuclei were stained with Hoechst 33342, as shown in blue fluorescence. Scale bar, 50 μm. Note that cultured astrocytes display process-bearing stellate cells under serum starvation, and change into polygonal morphology in response to S1P. (F) Quantification of the percentage of polygonal cells in the presence or absence of the indicated drugs. ***$P < 0.001$ vs. control (n = 3–5).

Fig. 4. S1P-induced astrocytic migration in cultured rat astrocytes. Astrocytic migration was measured by scratch-wound assay. Astrocytes were treated with FBS (0%) (control) or the indicated drugs for 72 h following serum starvation. Representative photographs were obtained at 0 and 72 h. The areas of astrocytic migration were normalized to that of the control cells grown in EMEM containing FBS (10%) for 72 h. The depicted area of migration is representative of three independent experiments performed in 4–8 wells in one experiment. Scale bar, 100 μm.

Fig. 5. Changes in mRNA expression levels and CXCL1 release into astrocyte culture medium 24 h after S1P treatment.

(A-H) mRNA levels of BDNF (A), GDNF (B), NGF (C), COX2 (D), ICAM1 (E), IL6 (F), CCL5 (G), and CXCL1 (H) in rat primary astrocytes that received control treatment or S1P (1 μM) for 24 h. *P < 0.05 vs. control (n = 4–7). (I) CXCL1 release in the astrocyte culture medium was measured by ELISA assay. Astrocytes were treated with control media, S1P (1 μM), S1P and $S1P_1$ antagonist VPC44116 (VPC; 1 μM), S1P and $S1P_2$ antagonist JTE013 (JTE; 1 μM), or S1P and $S1P_3$ antagonist CAY10444 (CAY; 10 μM). *P < 0.05, ***P < 0.001 vs. control, ###P < 0.001 vs. S1P alone (n = 4).

Fig. 6 Involvement of TRPC6, Ca^{2+} signaling, and the MAPK pathways in S1P- induced CXCL1 release.

(A) S1P-induced activation of MAPK pathways. Astrocytes were treated with control media or 1 μM S1P for 10 min (p38) or 30 min (ERK, JNK). Cell lysates were immunoblotted for phosphorylated MAPK proteins (p-ERK, p-JNK, p-p38) or total MAPK proteins (t-ERK, t-JNK, t-p38). Each value is expressed as the ratio of the phosphorylated MAPK protein level to the corresponding total MAPK protein level and the control value was set to 1. *P < 0.05 vs. control (n = 3-5). (B-E, J,O) Astrocytes were treated with control media, S1P (1 μM), S1P and MEK inhibitor PD98059 (PD; 30 μM), JNK inhibitor SP600125 (SP; 30 μM), or p38 inhibitor SB203580 (SB; 30 μM) (B), S1P and Pyr2 (1–10 μM) (C), S1P and Pyr3 (1–10 μM) (D), S1P and

PKC inhibitor bisindolylmaleimide I (BIM; 1 μM), endoplasmic reticulum Ca^{2+}-ATPase inhibitor CPA (30 μM), or intracellular Ca^{2+} chelator BAPTA-AM (3 μM) (E), or OAG (1-100 μM) (J). CXCL1 release in the astrocyte culture medium was measured by ELISA assay. ***P < 0.001 vs. control, #P < 0.05, ###P < 0.001 vs. S1P alone (n = 4-5). (F) TRPC6 mRNA expression in astrocytes treated with control siRNA or siRNA for 72 h. ***P < 0.001 vs. control siRNA (n = 8–9). (G, H) Representative traces of Ca^{2+} responses to OAG (100 μM) in astrocytes treated with control siRNA (G) or TRPC6 siRNA (si-TRPC6) (H) for 72 h. (I) Percentages of astrocytes treated with siRNA or si-TRPC6 that respond to OAG (100 μM) treatment for 10 min. *P < 0.05 vs. control siRNA (n = 6–9). (K-N) Representative traces (K, L) and quantitative data of peak Ca^{2+} amplitude (M) and sustained Ca^{2+} concentration (N) due to S1P (1 μM) in astrocytes treated with control siRNA (K, M, N) or si-TRPC6 (L-N) for 72 h. *P < 0.05 vs. control siRNA (n = 4). (O) CXCL1 release from astrocytes treated with siRNA or si-TRPC6 for 72 h after 24 h of control treatment or S1P (1 μM). ***P < 0.001 vs. control siRNA-treated control, ###P < 0.001 vs. control siRNA-treated S1P (n = 5).

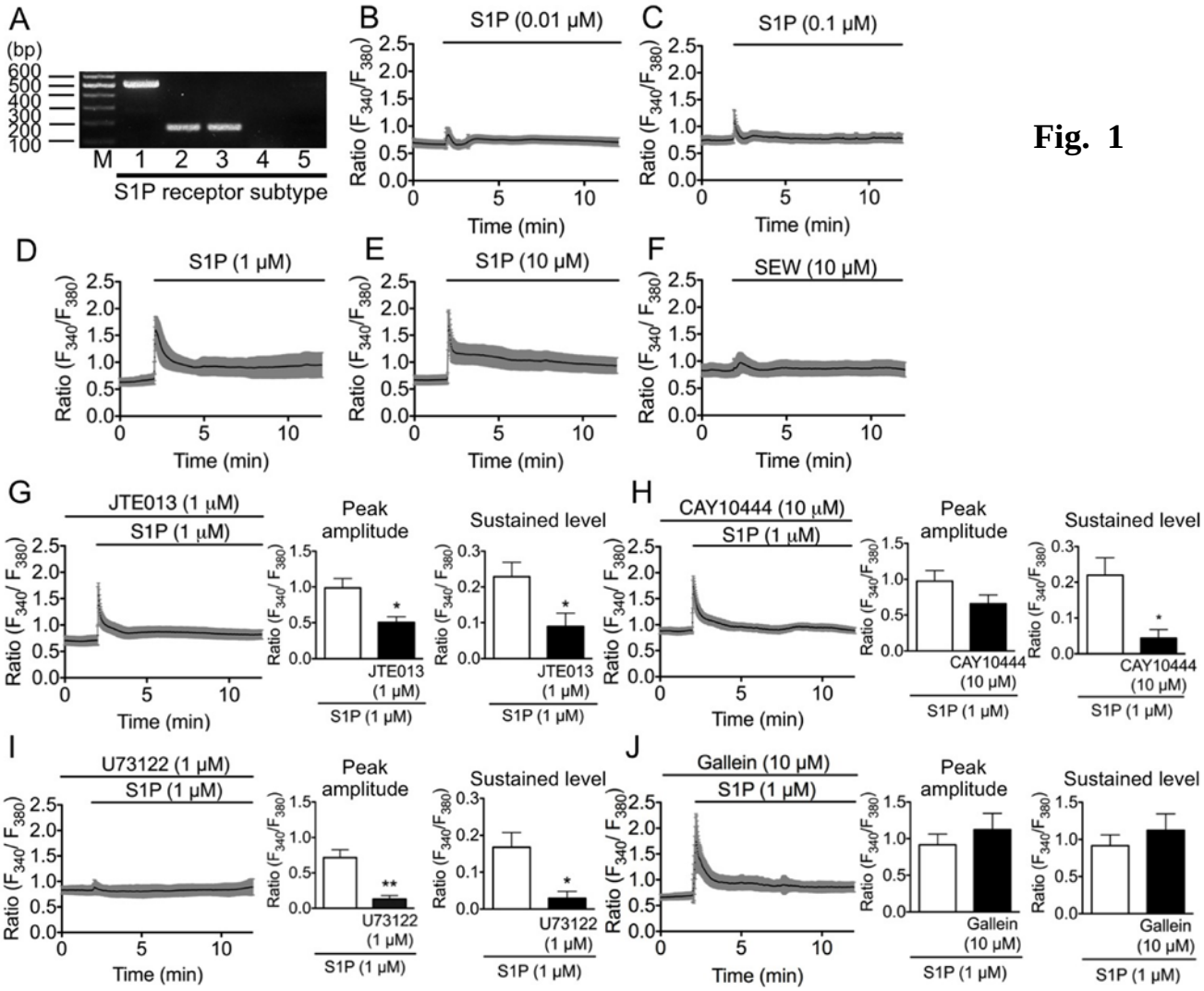

Fig. 1

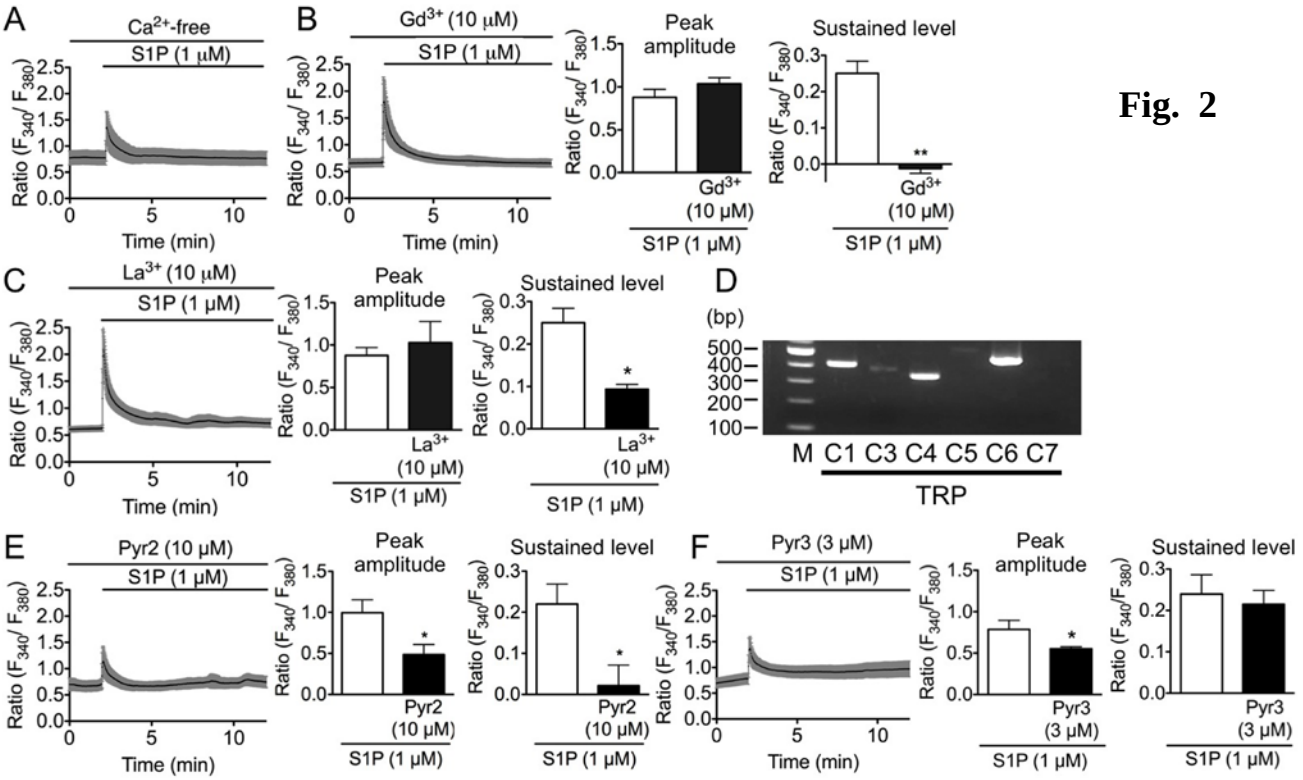

Fig. 2

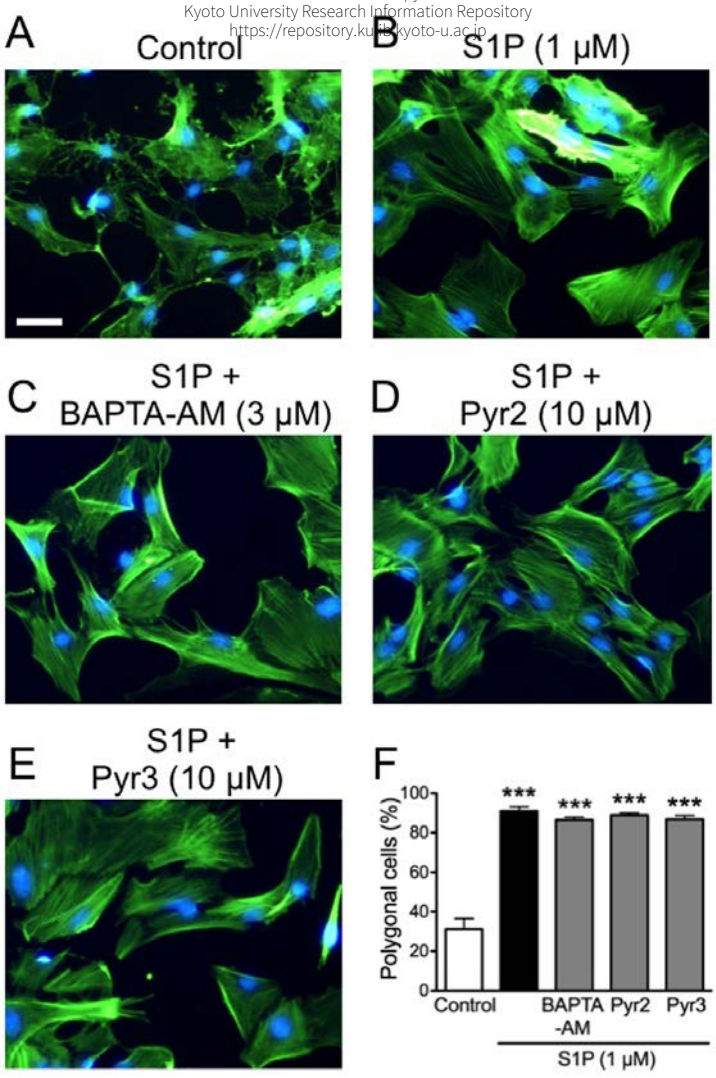

Fig. 3

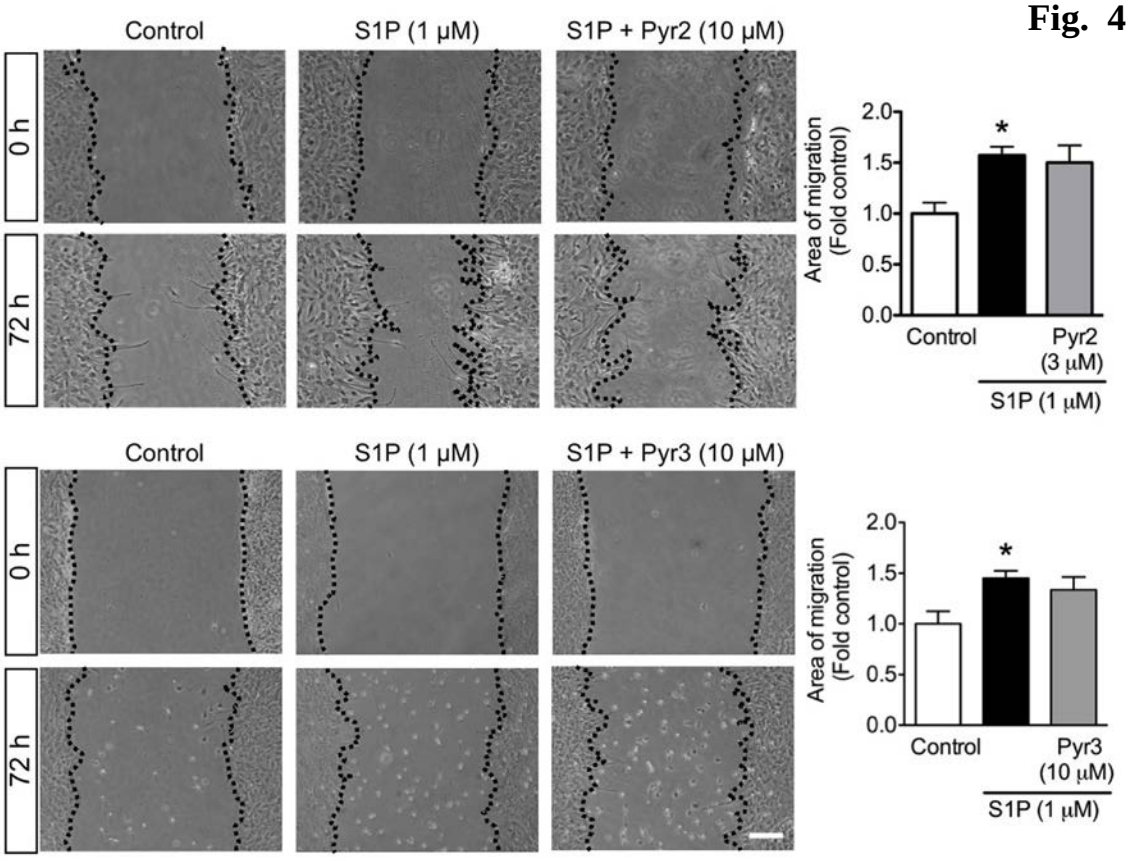

Fig. 4

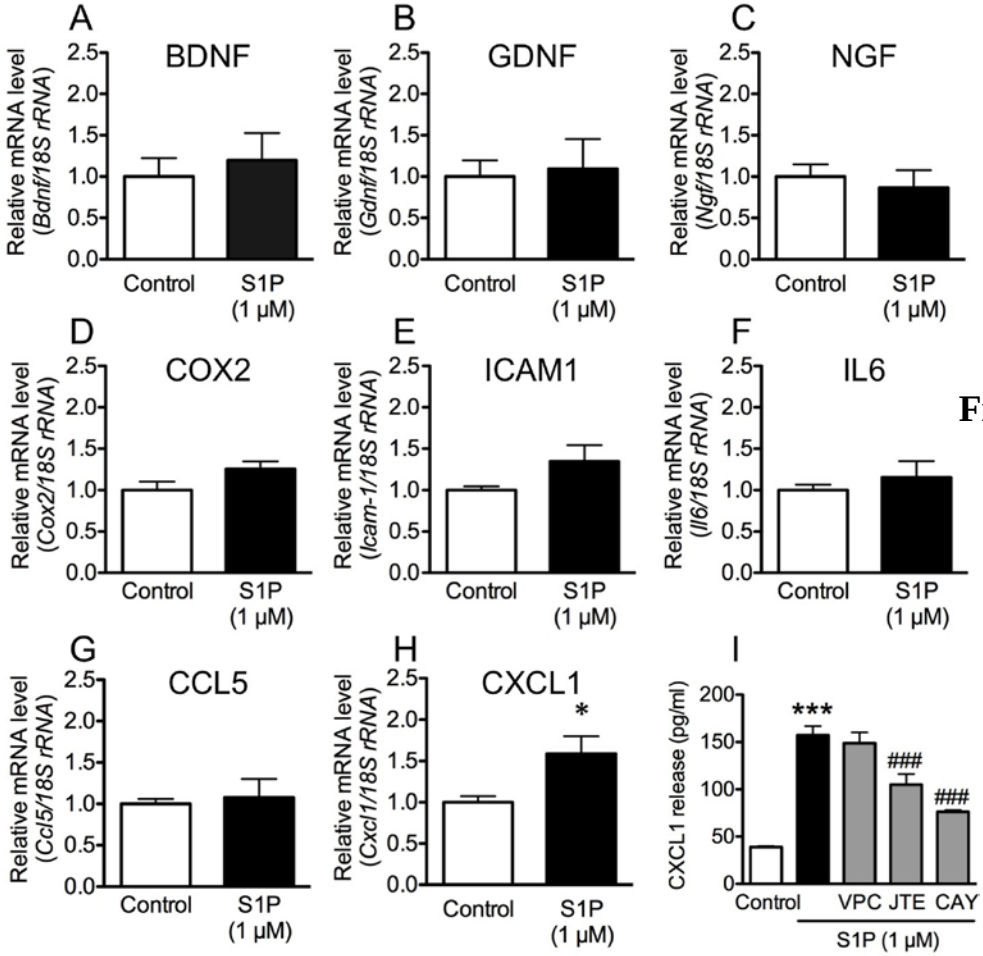

Fig. 5

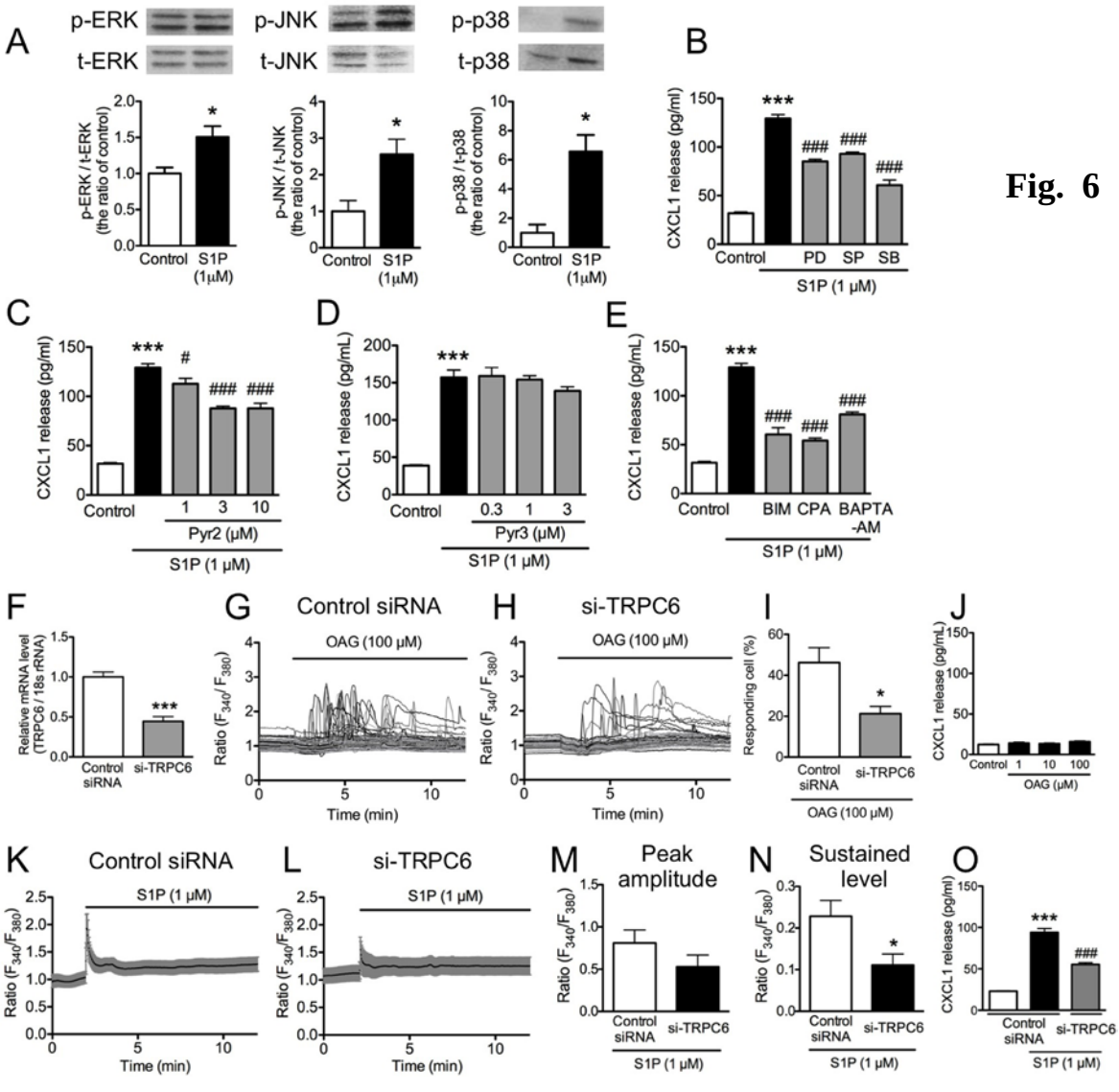

Fig. 6